



Efficient Delivery of Recombinant Human Bone Morphogenetic Protein (Rhbmp-2) With Cockle Shell Derived Calcium Carbonate Nanoparticles (CaCO₃NPs)

Ataa T. Ghazi ⁽¹⁾
Hayder F. Saloom ⁽²⁾
Rana I. Mahmood ⁽³⁾ *

⁽¹⁾ Department of Orthodontics, College of Dentistry, University of Baghdad, Baghdad, Iraq.

⁽²⁾ P.O.P. Department, College of Dentistry, Mustansiriya University, Baghdad, Iraq.

⁽³⁾ Dep. of Biomedical Engineering, College of Engineering, Al-Nahrain University, Baghdad, Iraq.

Keywords:

Orthodontics, CaCO₃NPs, rhBMP-2, drug delivery, fibroblast.

Article Info.:

Article History:

Received: 26/1/2023

Received in revised form:
30/1/2023.

Accepted: 31/1/2023

Final Proofreading:
31/1/2023

Available Online: 1/12/2023

© THIS IS AN OPEN ACCESS ARTICLE
UNDER THE CC BY LICENSE

<https://creativecommons.org/licenses/by/4.0/>



Citation: Ghazi AT, Saloom HF, Mahmood RI. Efficient Delivery of Recombinant Human Bone Morphogenetic Protein (Rhbmp-2) With Cockle Shell Derived Calcium Carbonate Nanoparticles (CaCO₃NPs). Tikrit Journal for Dental Sciences 2023; 11(2): 216-231.

<https://doi.org/10.25130/tjds.11.2.8>

*Corresponding Author:

Email:

rana.i.mahmood@nahrainuniv.edu.iq

Dep. of Biomedical Engineering, College of Engineering, Al-Nahrain University, Baghdad, Iraq .

Abstract

Bone morphogenetic protein-2 (BMP-2) has a significant function in the formation of cartilage and bones. Notably, dosing of only BMP-2 protein intravenously is ineffective. Persistent transportation of the stabilized BMP-2 through a carrier has been seen to be essential for enhancing the osteogenesis impact of BMP-2. The current research built a new system of drug delivery by utilising cockle shell derived calcium carbonate nanoparticles (CaCO₃NPs) and studied the efficacy of the delivery system on the recombinant human bone morphogenetic protein (rhBMP-2). rhBMP-2-CaCO₃NPs nanoparticles were synthesised by means of a modest precipitation procedure along with mechanical grinding. Fourier-transform infrared spectroscopy, UV-Vis spectrophotometer, scanning electron microscope, X-ray powder diffraction, transmission electron microscope, and zeta potential were utilised for characterising the conjugated rhBMP-2-CaCO₃NPs. Cytotoxicity of rhBMP-2, CaCO₃NPs and rhBMP-2-CaCO₃NPs was studied by utilising methylthiazol tetrazolium assay against fibroblast (Rat-1) cells in comparison to rhBMP-2 and CaCO₃NPs. The outcomes signified bio-stability of CaCO₃NPs and lower toxicity for Rat-1 cells. In summary, CaCO₃NPs were prepared by a simple precipitation process. The ensuing nanoparticles could competently entrap rhBMP-2 and generated stable rhBMP-2-CaCO₃NPs. A sustained discharge of rhBMP-2 from the CaCO₃NPs was seen. CaCO₃NPs loaded with rhBMP-2 demonstrated reasonable bio-compatibility. The outcomes indicated that CaCO₃NPs may have significant ability as carrier of therapeutic proteins within bone tissue engineering.

Introduction:

Bone morphogenetic proteins (BMPs) are growth elements which stimulate cartilage, bone, and periodontal ligament (PDL) fibre development ⁽¹⁾. They function locally at the place of application, frequently assimilated in dried bone matrix and utilised for repairing defects. Their impacts on bone and the adjacent tissues are only provisional ⁽²⁾. The restorative impacts of BMPs have been bounded to the size of matrix and the BMP biological activity span. BMPs have been utilised in orthopaedic care ⁽³⁾, regenerative periodontal therapy ⁽⁴⁾, and oral surgical procedures ⁽⁵⁾. In orthodontics, preliminary research evaluated the function of BMPs in enhancing post orthodontic stability. Positive impacts on incisor integrity and revival of adjacent structures were noted. Notably, there's been indication of hypercementosis as well as localized fusion of root and alveolar bone, both of which might proceed to ankyloses ⁽⁶⁾. An animal model of orthodontic retention is essential for explaining the process of orthodontic relapse. Many experimental studies to investigate orthodontic tooth movement and relapse were conducted on monkey, dogs, sheep and rodent (rabbits, rats and mice); however, rats are the most commonly used as an animal model in this field, due to priority of it regarding size, handling, cheap and short bone remodelling cycle ^(7, 8). One bone remodelling cycle (sigma) of rats takes 10-31 days, depends on age. At 6 months of age, it takes approximately 21 days therefore in this study the active phase was kept 21 days in order to accommodate with bone metabolism for one remodelling cycle ⁽⁹⁾. Nanotechnology pertains to the use of material at the nanoscale level. Present studies in the domain of nanotechnology are drawing the attention of large firms and nations for investing in this swiftly growing field ^(10, 11). Material at nanometre scale make the most of novel physical, biological, and chemical attributes, which could alter or improve drug properties. Diverse types of nanoparticles for drug delivery functions

have been studied until now, especially in the intricate structures of teeth and bone ⁽¹²⁾. Calcium derivatives have been the most important natural components of teeth and bones. Actually, they are the primary tissue in bones. Osseous tissue majorly comprises a compound material involving the inorganic mineral calcium derivatives ⁽¹³⁾. Tooth enamel is among the four tissues, which constitute the tooth and it comprises the maximum percentage of minerals, typically calcium ⁽¹⁴⁾. Thus, diverse calcium derivatives have been observed to possess significant potential to be employed in ailments pertaining to teeth and bones because of their perfect biocompatibility with the natural teeth and bone structures along with biodegradability ⁽¹⁵⁾. Filling dental caries, curing of early dental caries lesions, and producing neo-formed bone tissue using various kinds of calcium derivatives has also signified noteworthy applications ⁽¹⁶⁾. A popular calcium derivative that has a notable history of use in diverse domains is calcium carbonate (CaCO_3). It was utilized in paint, plastics, inks, paper, food, and the pharmaceutical sector ^(15, 17). Medicinal uses of CaCO_3 in contemporary healthcare setups have drawn the focus of researchers because of its abundant potential and competency. This material is economical, accessible, safe, biocompatible, osteoconductive, and bio-restorative ^(14, 15). Moreover, because of the slow degradation and its sensitivity to pH, calcium carbonate can be utilized as a sustained release mechanism for preserving the drugs in the targeted sites for prolonged durations post dosing ⁽¹⁸⁾. A very common source of CaCO_3 is the cockle shell. It comprises around 96% CaCO_3 whereas other constituents are organic substances and other oxides, such as MgO , SiO_2 , and SO_3 ⁽¹⁹⁾. Based on the earlier studies, it was suggested that the CaCO_3 derived from cockle shell can be employed as good alternative biomaterial for bone substitution in organising bone defects ⁽²⁰⁾. Nowadays, CaCO_3 nanoparticles have attracted an interest among researchers for therapeutic applications. They are found in 3 common polymorphs: aragonite, vaterite, and calcite ⁽²¹⁾. Aragonite is a naturally

occurring carbonate mineral ⁽²²⁾. It is the latest artificial nanoparticles which have arisen as the most widespread targets by researchers for deep investigation in different domains, particularly in bone tissue design, as well as biomedical and pharmaceutical sciences ⁽²³⁾. CaCO₃-based materials possess biocompatibility and biodegradability properties, which prove to be ideal to function as a smart carrier to transport drugs, enzymes, and genes ^(24, 25). This research aimed to study the CaCO₃NP efficacy on retention phase, which is followed by active orthodontic tooth movement to function as a “Biological Retainer”. Via measuring stability and relapse after orthodontic tooth movement using rat model.

Materials And Methods:

Synthesis of CaCO₃NPs

Microscale Synthesis of CaCO₃NPs Powder

Distilled water was used to wash cockle shells, which were boiled for nearly 30 minutes using a steel vessel, followed by oven drying (UM500, Memmert GmbH+ Co.KG, Schwabach Germany) at 55°C. Subsequently, 100 ml solution of a cleaning agent mixed with distilled water (ratio 1:2) was used to rinse dried shells to eliminate stains and debris. A pulverising blender ground the shells to powder form. The powdered cockle shells were filtered using a laboratory-grade steel sieve having a 90 µm aperture, followed by a second steel sieve with a finer 75 µm aperture. Subsequently, micrometre-level CaCO₃NPs powder was maintained at 50°C inside an oven before additional treatment ^(25, 26).

Nanoscale Synthesis of CaCO₃NPs

CaCO₃NPs were produced using a straightforward mechano-chemical process followed by simple precipitation. Two grams of ground CaCO₃NPs powder comprising 75 µm particles was mixed with 100 ml deionised water; subsequently, 0.5 ml BS-12 was mixed. A magnetic stirrer was tuned at 1,000 rpm and two hours to blend the solution at 27°C. Filter paper (Filtres Fioroni, Ingré, France) was used to clean the aqueous

solution. Deionised water was used several times to rinse the filter paper to eliminate the BS-12 residue. The sediment residue on the filter paper comprised nanoparticles that were dried at 50°C for 72 hours using an oven. The synthesised dry nanocarriers were processed further using an 8 cm diameter cylindrical glass jar. Seven ceramic balls were placed inside the container, and the apparatus was rolled on a ball miller for five days at 200 rpm. The CaCO₃NPs powder was placed inside glass bottles that were maintained in an oven at 50°C ⁽²⁷⁾.

Preparation of rhBMP-2 Loaded CaCO₃NPs (rhBMP-2- CaCO₃NPs)

The approach suggested by (Hamidu *et al.*, 2019, and Mailafiya *et al.*, 2021) was adopted with some changes to load CaCO₃NPs (27, 28). A mixture was created using 1 mg rhBMP-2, 15 mg CaCO₃NPs, and 3 ml deionised water. This mixture was placed in a dark environment and stirred overnight. It was subsequently subjected to 20,000 rpm centrifugation, followed by deionised water rinsing and oven drying at 25°C. CaCO₃NPs were evaluated for drug loading and encapsulation efficiency by calculating the difference between the overall protein feed and non-trapped protein levels in the liquid suspension per unit of CaCO₃NP weight. Triplicate measurements with distinct values helped determine CaCO₃NPs encapsulation efficiency (EE%) and product loading capacity (PLC%); the following expressions were used:

PLC%

$$\text{PLC\%} = \frac{\text{Mass of rhBMP-2 loaded to the CaCO}_3\text{NPs}}{\text{Mass of CaCO}_3\text{NPs} - \text{Mass of CaCO}_3\text{NPs}} \times 100 \quad (1)$$

EE%

$$\text{EE\%} = \frac{\text{Mass of rhBMP-2 loaded to the CaCO}_3\text{NPs} - \text{Mass of CaCO}_3\text{NPs}}{\text{Mass of CaCO}_3\text{NPs}} \times 100 \quad (2)$$

The first mass of rhBMP-2 used to the CaCO₃NPs

These equations were modified from a prior work (29).

Characterization of CaCO₃NPs Nanoparticles

Absorbance Spectroscopy

The required rhBMP-2, CaCO₃NPs, and rhBMP-2- CaCO₃NPs specimens were assessed using a UV-Vis spectrophotometer (1650PC, Shimadzu Europe, Duisburg, Germany) at a 1 cm cuvette path length. Samples were examined from 200 nm to 800 nm against the reference buffer.

Fourier Transform Infrared Spectroscopy (FT-IR)

Functional group endings of the rhBMP-2, CaCO₃NPs and rhBMP-2-CaCO₃NPs were determined using Fourier Infrared spectrophotometer (FT-IR) at a scale of 4000 cm⁻¹ to 400 cm⁻¹ with a resolution of 2 cm⁻¹ and an average scan of 64 times.

Powder X-Ray Diffraction

The crystallization and purity characteristics of unconjugated rhBMP-2, CaCO₃NPs, and rhBMP-2- CaCO₃NPs samples were assessed using a Rigaku XRD. Traverse parts were set on a quartz plate in order to interact with 1.5406 Å wavelength Cu K α radiation. The specimens were assessed at intensity and diffraction angle values between 2° to 80° to produce distinct patterns of Rat-1 lection peaks. The experiment has been carried out at room temperature, for a 2 θ range of 4-50°C, 0.6°/min scanning speed, and 2 θ =0.02° sampling interval.

SEM and TEM Scanning of CaCO₃NPs and rhBMP-2- CaCO₃NPs

Field-emission scanning electron microscopy was used to evaluate the morphological characteristics of CaCO₃NPs. The equipment was set at 30 mA at 200 kV; moreover, a high-resolution transmission electron microscopy was used at 5 kV.

SEM specimen preparation was done by placing the material on an aluminium plate coated with gold using sputter coating in an argon atmosphere. Both CaCO₃NPs and rhBMP-2- CaCO₃NPs were mixed in 90% ethanol, followed by 30 min of sonication. One

drop of both specimens was put on a carbon-coated copper grid, and kept at room temperature for drying before TEM assessment⁽³⁰⁾.

Determination of Zeta Size, Potential and Polydispersity Index (PDI)

Zetasizer Nano ZS, Malvern Tools was employed to determine PDI (polydispersity index), nanoparticle size, and surface charge. The test mixture comprised 0.4 mg of CaCO₃NPs and rhBMP-2- CaCO₃NPs dissolved in 12 ml deionised water sonicated for 30 minutes. Then, the buoyant material was placed in a basin for examination as per the technique used by⁽³⁰⁾. Observations were taken in triplicate without concentration changes; a 90° scatter angle and 25 °C temperature were used.

The Drug Release Study

Release characteristics of rhBMP-2 were established. Individual dialysis containers (MWCO: 12 kDa) were loaded with rhBMP-2-CaCO₃NPs specimens (1 mg rhBMP-2-CaCO₃NPs in 1 ml solution) and placed inside 50 mL PBS having 4.6 and 7.6 pH values. A magnetic stirrer was used for the tubes, and the release assessment was commenced by 100 rpm stirring at 37°C. Around 1 ml buffer solution was extracted from the tubes and replenished with an equivalent amount of fresh phosphate solution at particular periods. The extracted solution was used for analysis (0, 0.5, 2, 3, 6, 12, 24, 48, and 72 hours). The concentration of rhBMP-2 release was measured using UV/Vis spectrophotometry at 280 nm on the samples⁽²⁵⁾.

Maintenance of cell cultures

$$\text{Cytotoxicity} = \frac{A-B}{A} * 100$$

Where A and B are the optical density of control and the optical density of test

RPMI-1640 was used to store Rat-1 cells mixed with 100 units/mL penicillin, 100 µg/mL streptomycin, and 10% foetal bovine serum. Trypsin-EDTA was used

for cell transfer; replantation was conducted twice a week at 80% confluence, while incubation was conducted at 37°C^(31, 32).

Biocompatibility

An MIT assay was implemented using 96-well plates to determine the cytotoxic characteristics of rhBMP-2, rhBMP-2-CaCO₃NPs, and CaCO₃NPs⁽³³⁾. The well was seeded with cells at 1 × 10⁴ cells/well. A well-defined monolayer was built in 24 hours and the cells were processed using various concentrations of the testing substances. The medium was separated for 72 hours to prepare for cell viability assessment. 28 μL MTT at 2 mg/mL concentration was employed for cell incubation performed for 2.5 h at 37°C. After MTT medium removal, 130 μL of DMSO (Dimethyl Sulphoxide) was used to dissolve the crystals inside the wells). Subsequently, the sample was incubated for 15 min at 37°C with shaking⁽³⁴⁾. Absorbance properties were determined through a 492 nm configured microplate instrument; specimen evaluation was done in triplicate. Cell growth inhibition rate was determined using the following formula^(11, 35).

$$\text{Inhibition rate} = A - B/A * 100$$

where A is the optical density of control and B is the optical density of the samples⁽³⁶⁾. Cell shape was visualised using an inverted microscope; 24-well micro-titration plates were seeded at 1×10⁵ cells/mL density, followed by 24 h incubation at 37°C. Next, cell treatment was performed for 24 h using rhBMP-2, CaCO₃NPs, and rhBMP-2-CaCO₃NPs. The plates were then stained using crystal violet, followed by 10-15 mins incubation at 37°C⁽³⁷⁾. The dye stain was slowly removed by rinsing with tap water. Cells were evaluated using an inverted microscope configured to 100x magnification. A digital camera attached to the microscope recorded the images^(38, 39).

Statistical analysis

GraphPad Prism 6 was used to conduct an unpaired t-test to statistically test the gathered data (40). The outcomes were

based on triplicate measurements: mean ± SD were reported⁽⁴¹⁾.

Results And Discussion:

Characterization of CaCO₃NPs Nanoparticles

A-UV-Vis adsorption spectra

A UV-Vis spectrophotometer was used to identify the optical characteristics of rhBMP-2- CaCO₃NPs, rhBMP-2, and CaCO₃NPs. Fig.(1) depicts the UV absorption characteristics. The band points specific to 205 and 265 nm belong to nanoparticles of CaCO₃. The absorption coefficient α can be computed from the relation:

$$\alpha = 2.303 \frac{A}{t}$$

where A is the absorbance and t is the thickness of the cuvette. The optical band gap of the nano-powders was ascertained by applying the Tauc relationship as stated by⁽⁴²⁾:

$$ah\nu = A(h\nu - E_g)^n$$

Here, h is Planck's constant, ν is the photon frequency, E_g is the optical band gap, A is a constant, and n = 2 for indirect band gap insulator.

The linear area of $(ah\nu)^{1/2}$ vs photon energy ($h\nu$) on the Y- and X-axes, respectively, is extrapolated to identify the 5.62 eV optical band gap (E_g) for bulk CaCO₃NPs, rhBMP-2, and rhBMP-2-CaCO₃NPs. Moreover, the nanoparticle values were 5.36 eV (42 wt.% surfactant), 5.40 eV (36 wt.% surfactant), and 5.60 eV (30 wt.% surfactant), as depicted in Fig. (1). The band gaps computed for rhBMP-2- CaCO₃NPs, rhBMP-2, and CaCO₃NPs nano-powder samples were below the corresponding bulk values, indicating gradual blue shift; these observations align well with the band gaps computed previously by⁽⁴³⁾.

B-SEM and TEM Scanning of CaCO₃NPs and rhBMP-2- CaCO₃NPs

The size distribution, shape, and surface morphology of CaCO₃NPs, rhBMP-2, and rhBMP-2-CaCO₃NPs were analyzed by SEM and TEM. Results in Fig.(2) show the representative SEM images with the corresponding size distribution.

CaCO₃NPs appeared as homogenous uni-dimensional spherical nanoparticles with an average particle size of 54.74 ± 6.17 nm. Loading rhBMP-2 on CaCO₃NPs improves the spherical uniformity and dispersion of nanoparticles without affecting the size range. A rhBMP-2-CaCO₃NPs showed a round shape and particle size within the nanoscale range (92.12 ± 25.1 nm). Images of TEM Fig.(3A) confirmed the individual round shape of CaCO₃NPs in nanosized range 43.008 ± 9.72 nm, while Fig.(3B), clearly illustrates the spherical morphology of rhBMP-2-CaCO₃NPs with porous characteristics, in which the overall morphology regarding size, shape and dispersion verified the homogeneity of rhBMP-2 loaded CaCO₃NPs with an average size distribution of 62.73 ± 9.70 nm.

C-Fourier Transform Infrared Spectroscopy (FT-IR)

The FT-IR spectra of rhBMP-2, CaCO₃ NPs and rhBMP-2-CaCO₃NPs included bands range between 4000 - 400 cm⁻¹ was detected. The peaks of the three samples were matched with each other, revealing that the purity of CaCO₃ NPs was unaffected by the nanoscale forming protocol using BS-12, and the rhBMP-2 was well conjugated with CaCO₃ NPs, forming rhBMP-2-CaCO₃NPs complex. CaCO₃ NPs absorption peaks (3405.38, 2933.85, 2523.46, 1789.24, 1481.51, 1052.24, 850.42 and 709.85 cm⁻¹) showed a slight shift in their spectra, which may attributed to the binding between rhBMP-2 and the CaCO₃ NPs. Furthermore, functional group peaks were entirely unchanged Fig.(4).

D-X-Ray Powder Diffraction (XRD)

Moreover, an XRD analytical setup was used to extensively assess and record nanoparticles' crystalline phase. The absorption peak had a high density, clearly suggesting no changes to the crystalline array arrangement after rhBMP-2 addition Fig.(5).

The crystallinity of nanoparticles was excellently assessed and monitored using an XRD analysis system. The strong absorption peak strongly suggests that the

crystalline array fashion of CaCO₃NPs remained stable also after rhBMP-2 loading. The drug loading content and loading efficiency are critical factors in determining NPs' suitability as a drug delivery system ^(44, 45).

E-Determination of Zeta Size, Potential and Polydispersity Index (PDI)

Samples of rhBMP-2-CaCO₃NPs and CaCO₃NPs were tested using zeta potential assessment comprising intensity-specific size distribution, stability, and surface charge evaluation. A -7.95 ± 4.06 mV negative charge was indicated for CaCO₃NPs; moreover, the loaded rhBMP-2-CaCO₃NPs samples had a reduced distribution of zeta potential, comprising particles with -5.74 ± 5.82 mV negative charge Fig.(6).

Naturally produced CaCO₃NPs of aragonite polymorph can be suitably obtained using Cockle shells ⁽⁴⁶⁾. CaCO₃NPs have several uses for human ventures ⁽⁴⁶⁻⁴⁸⁾; additional innovations can be facilitated using nanotechnology. Nanotechnology offers numerous possibilities and benefits concerning medical advancement by increasing the efficiency of pharmaceutical products ⁽⁴⁹⁾. Using nanotechnology to produce CaCO₃NPs from natural materials provides numerous advantages. Nature-identical aragonite crystals are developed, and most of the distinct characteristics are retained ^(46, 50). SEM Fig.(2) and TEM Fig.(3) were used to uncover CaCO₃NPs morphologies in plain and rhBMP-2 loaded forms. Free CaCO₃NPs have a consistent nanoscale spherical geometry. Images suggest that the manufactured CaCO₃NPs were porous, increasing the applicability of physical adsorption-based drug loading. Loading rhBMP-2 did not significantly alter CaCO₃NPs morphology, except for a minor size distribution enhancement. The nanoparticles were examined thoroughly in their crystalline phase and assessed using the XRD analytical approach. The strong absorption peak suggests that the CaCO₃NPs crystalline structure does not change even after rhBMP-2 loading. Loading efficiency and drug amount are critical aspects to assess NP usability for drug delivery ^(44, 45).

F-The Drug Release Study

CaCO₃NPs were impregnated with the rhBMP-2 mixture and constantly stirred to load rhBMP-2 onto the nanoparticles. Here, the produced cores' pores can be filled by drug molecule infiltration or physical adsorption. This experiment yielded up to 92.3% loading efficiency, while the sample yielded 31.45% loading content after overnight stirring. Fig.(7) depicts the rhBMP-2-CaCO₃NPs release characteristics observed for 70 h using PBS with a 7.6 pH value. Rapid rhBMP-2 release was observed: $29.8 \pm 3.5\%$ and $52.8 \pm 2.9\%$ after 24 and 80 hours.

Biocompatibility

Cell viability

MTT assay was carried out to evaluate the biocompatibility of CaCO₃NPs, rhBMP-2, and rhBMP-2-CaCO₃NPs after 24 hrs of incubation with different concentration include (1.56, 3.10, 6.25, 12.50, 25.00, 50.00, 100.00, 200.00, 400.000 µg/ml). The toxicity of CaCO₃NPs, rhBMP-2, and rhBMP-2-CaCO₃NPs on Rat-1 cell showed almost the same impact on Rat-1 cell and increased in a dose-dependent way as shown in Fig.(8) While the maximum toxicity was recorded in group treated with 400 µg/ml of rhBMP-2-CaCO₃NPs.

Morphological changes of treated cells

The outcomes indicated that CaCO₃NPs were biocompatible and had low toxicity concerning RAT-1 cells at strong concentration levels of 400 µg/ml, while there was 80% or higher cell viability, indicating CaCO₃NPs nano-carrier compatibility and insignificant toxicity Fig.(9). It was assumed that CaCO₃NPs were less toxic because of gravity sedimentation ⁽⁵¹⁾. We assert that CaCO₃NPs blanketed the surface of the cell, blocking oxygen and essential nutrients in the culture. Therefore, exposure to stronger concentrations (up to 400 µg/ml) reduced the viability of the cell; regardless, cell viability was still reliable. Moreover, cytotoxic assessments were performed for RAT-1 cells to

contrast rhBMP-2- CaCO₃NPs and free rhBMP-2. The cytotoxic effect of rhBMP-2 has been significantly decreased after rhBMP-2 loading with CaCO₃NPs.

The shape of Rat-1 cells treated with CaCO₃NPs, rhBMP-2, and rhBMP-2-CaCO₃NPs after 24 hrs of incubation with different concentration include (1.56, 3.10, 6.25, 12.50, 25.00, 50.00, 100.00, 200.00, 400.000 µg/ml) were visualized under an inverted microscope, suggesting that CaCO₃NPs and rhBMP-2-CaCO₃NPs didn't show significant effect on cells. The outcomes align with an existing study that reported insignificant effects of rhBMP-2 on cell viability concerning three oral squamous cell carcinoma cell lines and fibroblasts ⁽⁵²⁾.

Conclusions:

In short, the ionic cross-linking technique was used to create CaCO₃NPs, which could effectively trap rhBMP-2 to create stable rhBMP-2-CaCO₃NPs. CaCO₃NPs were consistently emitted by rhBMP-2. CaCO₃NPs mixed with RhBMP-2 offered the desired bio-compatibility. These outcomes indicate the immense potential of CaCO₃NPs as protein carrier material for therapeutic tissue bioengineering.

Abbreviations:

- Bone morphogenetic protein: BMP
- rhBMP-2: Recombinant human Bone morphogenetic protein-2: rhBMP-2
- Calcium carbonate nanoparticles: CaCO₃NPs

Author Contributions:

Conceptualization: A.T.G. and H.F.S.;
 Methodology: R.I.M., A.T.G., and H.F.S.;
 Software: R.I.M; Writing—original draft
 preparation: A.T.G.; Writing—review and
 editing: H.F.S ; Supervision: H.F.S; and
 Project administration: H.F.S.

Funding acquisition: All authors have read and agreed to the published version of the manuscript.

Funding: This research was supported by the College of Dentistry, Baghdad University, Baghdad – Iraq (Grant No 523).

Institutional Review Board Statement
 Not applicable.

Informed Consent Statement: No applicable.

Data Availability Statement: No applicable.

Acknowledgments: The authors are grateful to the College of Dentistry in Baghdad University for extending help and support to complete the project. o (A.T.G).

Conflicts of Interest: The authors declare no conflict of interest.

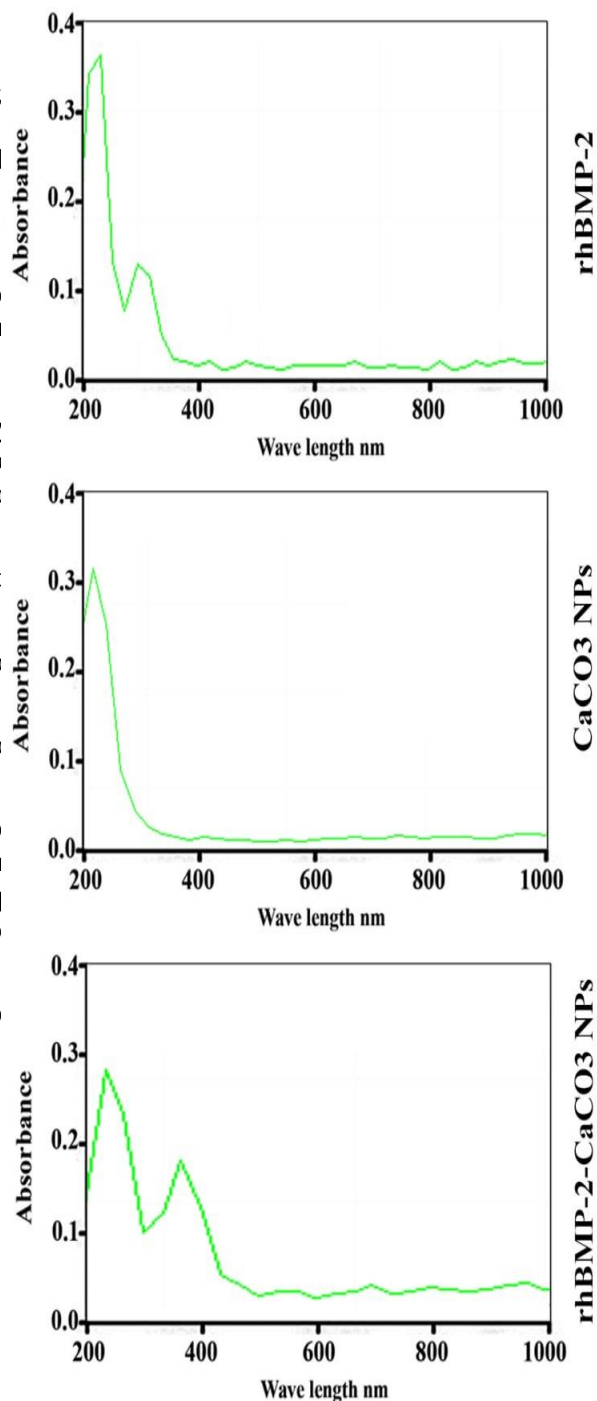
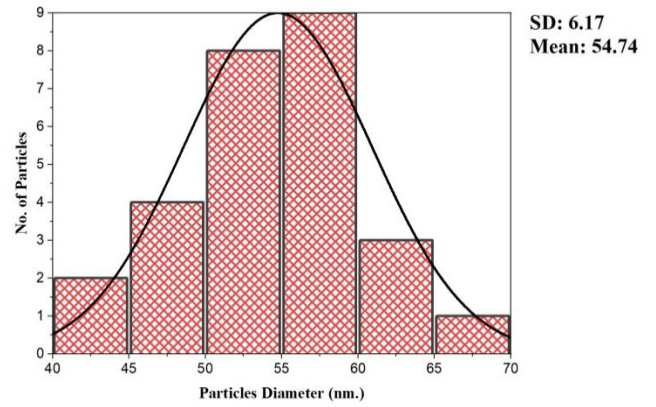
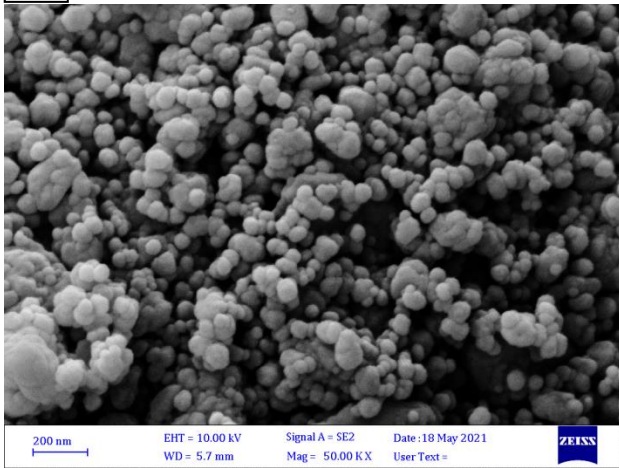


Fig. (1): Absorbance spectra of rhBMP-2, CaCO₃NPs, and rhBMP-2- CaCO₃NPs

A



B

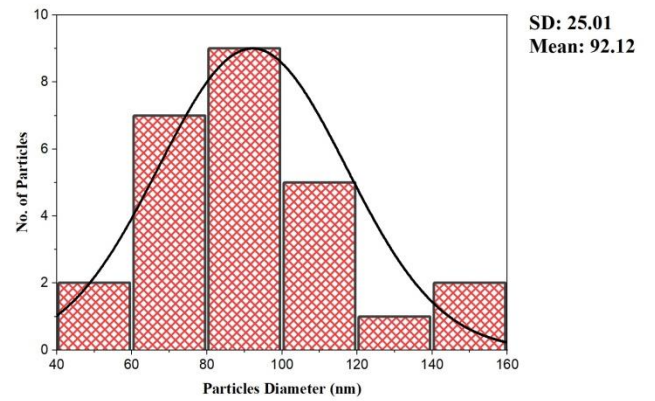
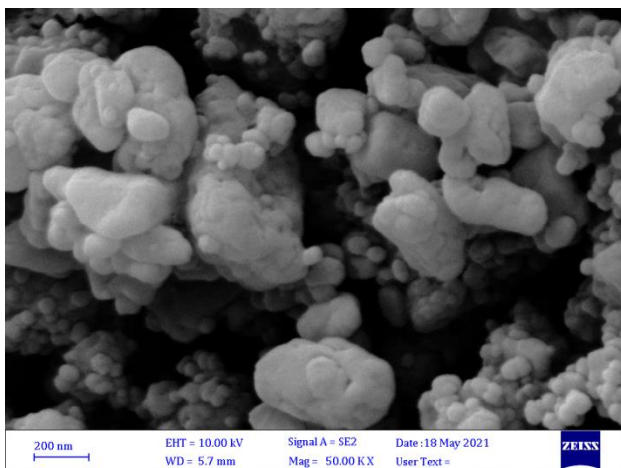


Fig. (2): Field-emission scanning electron microscopic morphologies of therapies with their corresponding particle size distribution histogram. A: CaCO₃ NPs. B: rhBMP-2-CaCO₃ NPs

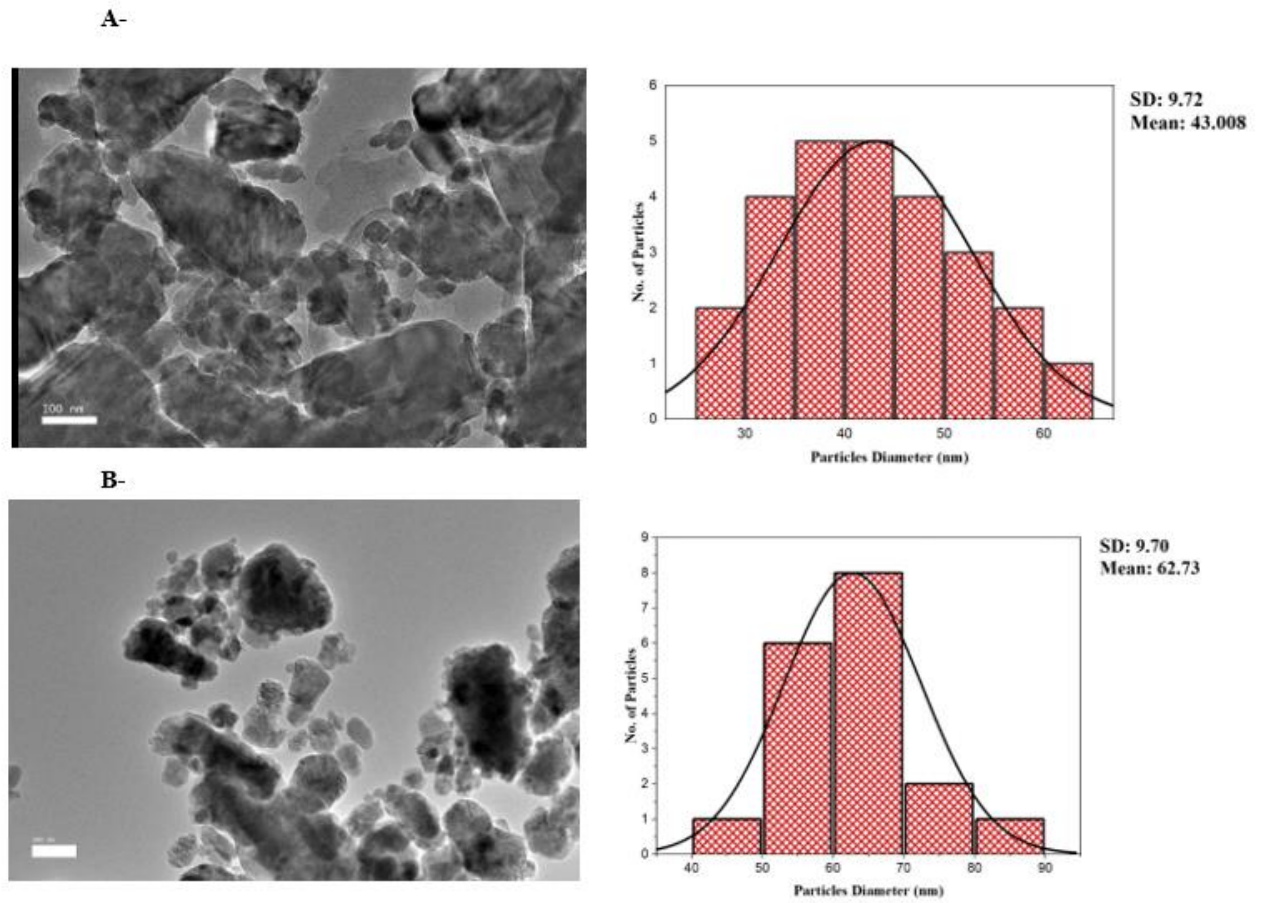


Fig. (3): High-resolution transmission electron microscopy of therapies with their corresponding particle size distribution histogram. A: CaCO₃ NPs. B: rhBMP-2-CaCO₃NPs.

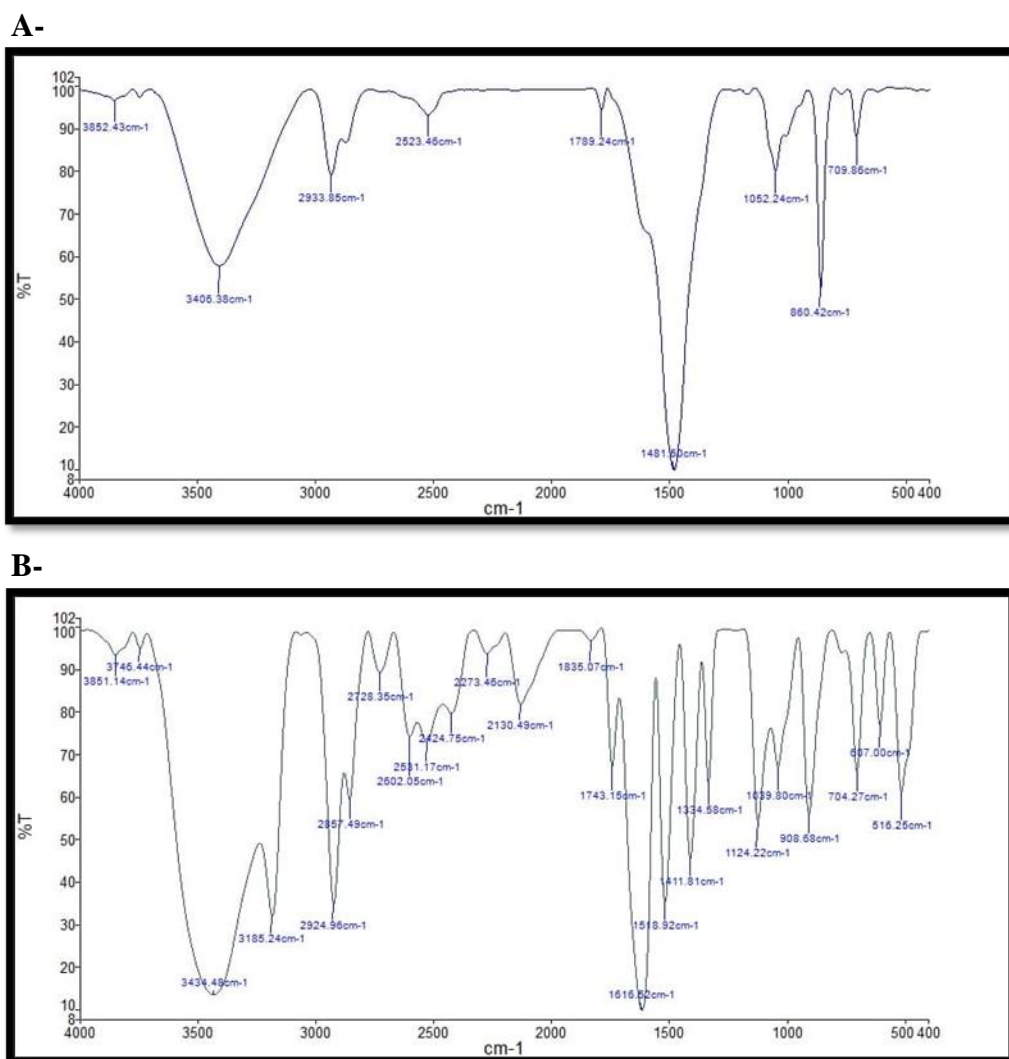


Fig. (4): FTIR. A- CaCO₃NPs. B- rhBMP-2- CaCO₃NPs

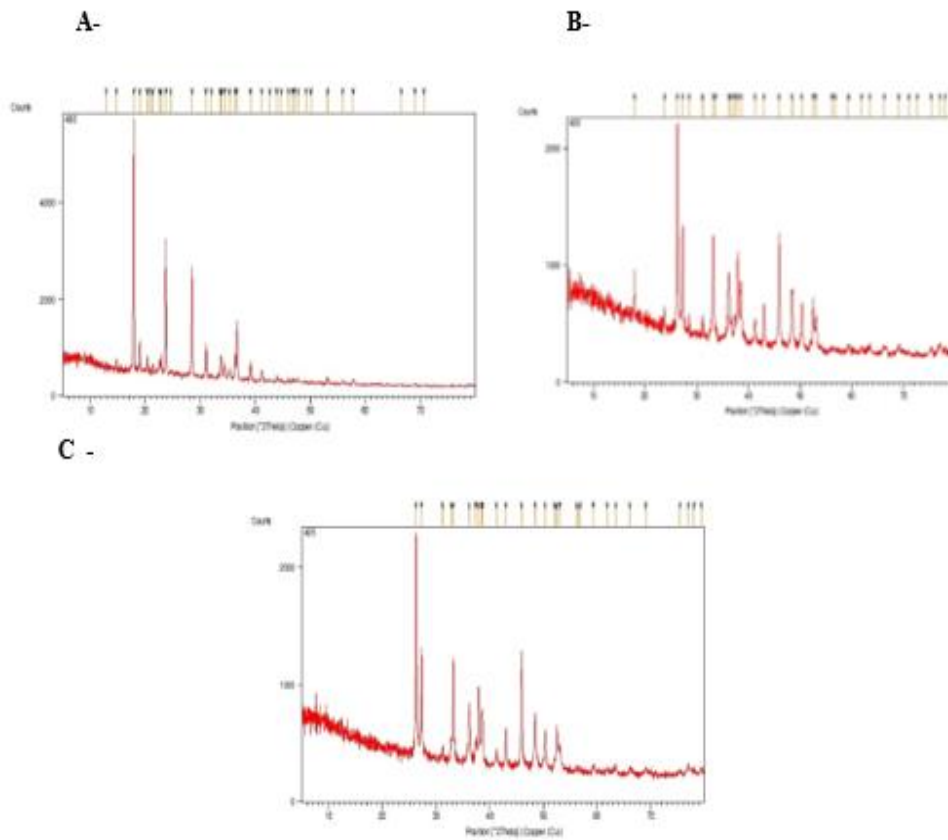


Fig. (5): XRD pattern of rhBMP-2, CaCO₃NPs, and rhBMP-2- CaCO₃NPs. Experiments performed at room temperature

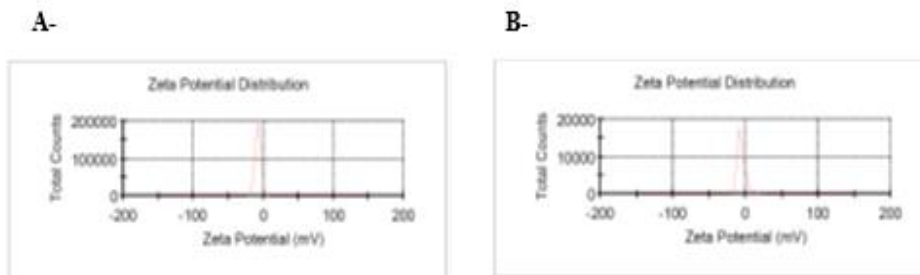


Fig. (6): Zeta potential; A- CaCO₃NPs. B- rhBMP-2-CaCO₃NPs

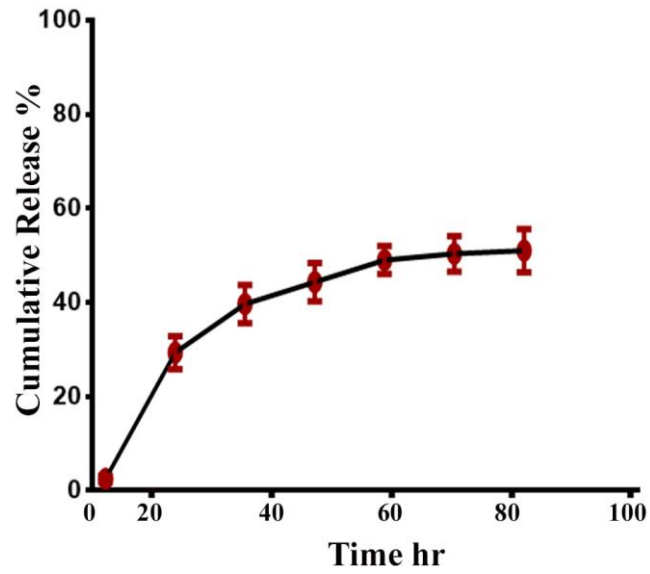


Fig. (7): The drug release study of rhBMP-2 was loaded into ACC- CaCO₃NPs.

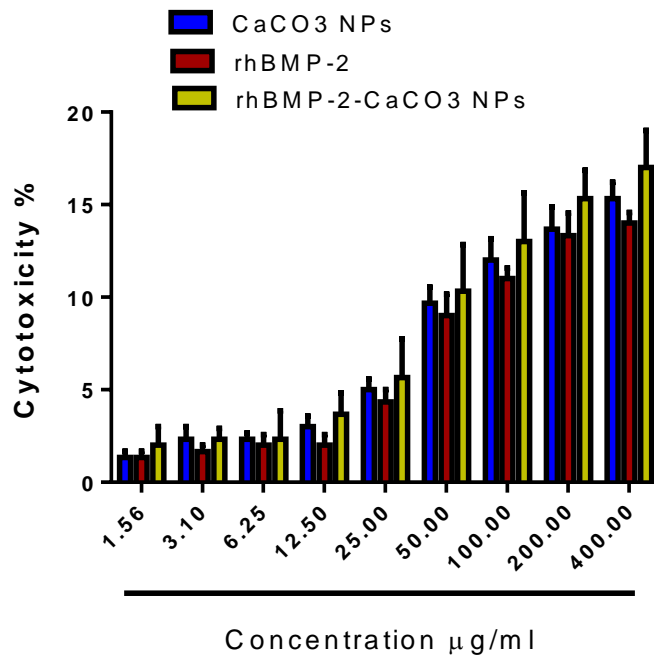


Fig. (8): Biocompatibility effect of CaCO₃NPs, rhBMP-2, and rhBMP-2-CaCO₃NPs in Rat-1 cells.

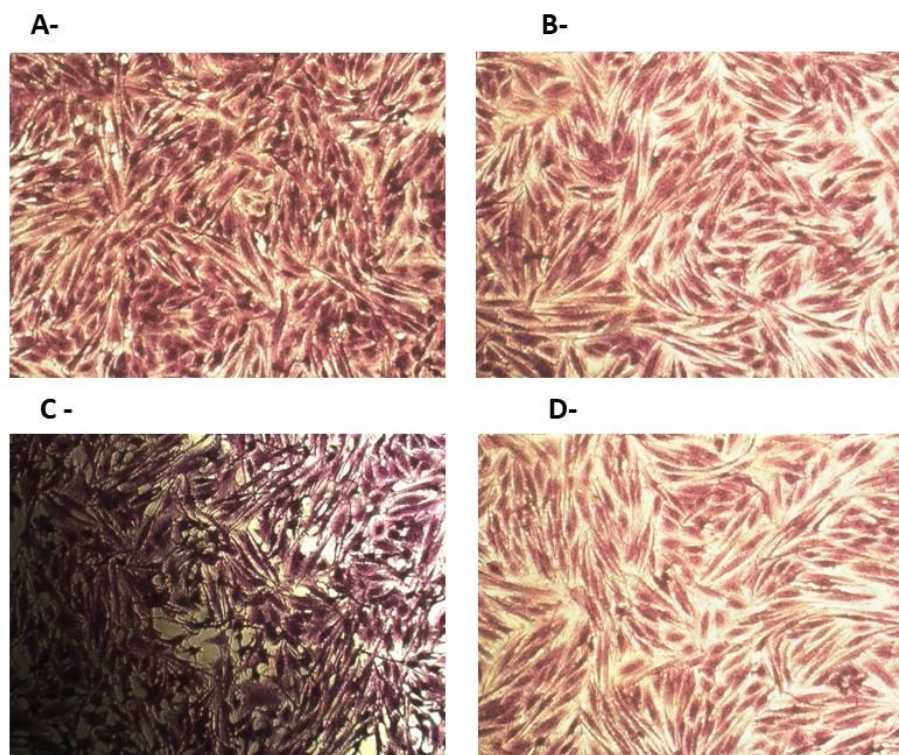


Fig. (9): A- Control untreated Rat-1 Cells B- Rat-1 cells treated with CaCO₃NPs C- Rat-1 cells treated with rhBMP-2 D- Rat-1 cells treated with rhBMP-2-CaCO₃NPs

References

1. Thorarinn J. Sigurdsson, Michael B. Lee, Kubota K, Thomas J. Turek, John M. Wozney, Wikesjö aUME. Periodontal Repair in Dogs: Recombinant Human Bone Morphogenetic Protein-2 Significantly Enhances Periodontal Regeneration. *J Periodontol.* 1995;66(2).
2. Sohei Ebara, Nakayama aK. Mechanism for the Action of Bone Morphogenetic Proteins and Regulation of Their Activity. 2002:S10-S5.
3. Safdar N Khan, Lane JM. The use of recombinant human bone morphogenetic protein-2 (rhBMP-2) in orthopaedic applications. *Expert Opin Biol Ther.* 2004;4(5):741-8.
4. Lee CT, Hum L, Chen YW. The effect of regenerative periodontal therapy in preventing periodontal defects after the extraction of third molars: A systematic review and meta-analysis. *J Am Dent Assoc.* 2016;147(9):709-19 e4.
5. Herford AS, Boyne PJ. Reconstruction of mandibular continuity defects with bone morphogenetic protein-2 (rhBMP-2). *J Oral Maxillofac Surg.* 2008;66(4):616-24.
6. Hassan AH, Al-Hubail A, Al-Fraidi AA. Bone inductive proteins to enhance postorthodontic stability. *Angle Orthod.* 2010;80(6):1051-60.
7. Ren Y, Jaap C Maltha AMK-J. The rat as a model for orthodontic tooth movement--a critical review and a proposed solution. *Eur J Orthod.* 2004;26(5):483-90.
8. Inoue K, Hara Y, Kuroda N, Sato T. Development of the oxytalan fiber system in the periodontal space of rat incisors. *Ann Anat.* 2013;195(5):475-83.
9. Baron R, Tross R, Vignery A. Evidence of sequential remodeling in rat trabecular bone: morphology, dynamic histomorphometry, and changes during skeletal maturation. *Anat Rec* 1984;208(1):137-45.
10. Al-Rahim AM, Mahmood RI, Mohammed MM, Omer DJGR. In vitro evaluation of antioxidant and cytotoxic activity of folate-methotrexate conjugated to bovine serum albumin nanoparticles against MCF-7, HepG2, and PC3 cell lines. 2022;29:101666.
11. Mahmood RI, Kadhim AA, Ibraheem S, Albukhaty S, Mohammed-Salih HS, Abbas RH, et al. Biosynthesis of copper oxide nanoparticles mediated *Annona muricata* as cytotoxic and

- apoptosis inducer factor in breast cancer cell lines. 2022;12(1):1-10.
12. Arias JL, López-Viota M, Gallardo V, Adolfin Ruiz MJDD, Pharmacy I. Chitosan nanoparticles as a new delivery system for the chemotherapy agent tegafur. 2010;36(6):744-50.
 13. Bandyopadhyay-Ghosh S. Bone as a collagen-hydroxyapatite composite and its repair. Trends in Biomaterials and Artificial Organs. 2008;22:112+.
 14. Hajime Ohgushi, Motoaki Okumura, Takafumi Yoshikawa, Keisuke Inoue, Norio Senpuku, Tamai aS. Bone formation process in porous calcium carbonate and hydroxyapatite. Journal of Biomedical Materials Research. 1992;26:885-95.
 15. Biradar S, Ravichandran P, Gopikrishnan R, Goornavar V, Hall JC, Ramesh V, et al. Calcium carbonate nanoparticles: synthesis, characterization and biocompatibility. J Nanosci Nanotechnol. 2011;11(8):6868-74.
 16. Hannig M, Hannig C. Nanotechnology and its role in caries therapy. Adv Dent Res. 2012;24(2):53-7.
 17. Ueno Y, Futagawa H, Takagi Y, Ueno A, Mizushima Y. Drug-incorporating calcium carbonate nanoparticles for a new delivery system. J Control Release. 2005;103(1):93-8.
 18. Qian K, Shi T, Tang T, Zhang S, Liu X, Cao Y. Preparation and characterization of nano-sized calcium carbonate as controlled release pesticide carrier for validamycin against *Rhizoctonia solani*. Microchimica Acta. 2010;173(1-2):51-7.
 19. Saidykhan L, Abu Bakar MZ, Rukayadi Y, Kura AU, Latifah SY. Development of nanoantibiotic delivery system using cockle shell-derived aragonite nanoparticles for treatment of osteomyelitis. Int J Nanomedicine. 2016;11:661-73.
 20. Shafiu Kamba A, Ismail M, Tengku Ibrahim TA, Zakaria ZA. A pH-sensitive, biobased calcium carbonate aragonite nanocrystal as a novel anticancer delivery system. Biomed Res Int. 2013;2013:587451.
 21. Salomão R, Costa LMM, Olyveira GMd. Precipitated Calcium Carbonate Nano-Microparticles: Applications in Drug Delivery. Advances in Tissue Engineering & Regenerative Medicine: Open Access. 2017;3(2).
 22. Sali SS. NATURAL CALCIUM CARBONATE FOR BIOMEDICAL APPLICATIONS. NAVI Mumbai: PATIL UNIVERSITY; 2015.
 23. Hammadi NI, Abba Y, Hezmee MNM, Razak ISA, Jaji AZ, Isa T, et al. Formulation of a Sustained Release Docetaxel Loaded Cockle Shell-Derived Calcium Carbonate Nanoparticles against Breast Cancer. 2017;34:1193-203.
 24. Ahmed H, Ajat M, Mahmood RI, Mansor R, Razak ISA, Al-Obaidi JR, et al. LC-MS/MS Proteomic Study of MCF-7 Cell Treated with Dox and Dox-Loaded Calcium Carbonate Nanoparticles Revealed Changes in Proteins Related to Glycolysis, Actin Signalling, and Energy Metabolism. Biology (Basel). 2021;10(9).
 25. Mahmood RI, Abbass AK, Al-Saffar AZ, Al-Obaidi JR. An in vitro cytotoxicity of a novel pH-Sensitive lectin loaded-cockle shell-derived calcium carbonate nanoparticles against MCF-7 breast tumour cell. Journal of Drug Delivery Science and Technology. 2021;61.
 26. Chemmalar S, Intan-Shameha AR, Abdullah CAC, Ab Razak NA, Yusof LM, Ajat M, et al. Synthesis and Characterization of Gefitinib and Paclitaxel Mono and Dual Drug-Loaded Blood Cockle Shells (*Anadara granosa*)-Derived Aragonite CaCO₃ Nanoparticles. Nanomaterials (Basel). 2021;11(8).
 27. Hamidu A, Mokrish A, Mansor R, Razak ISA, Danmaigoro A, Jaji AZ, et al. Modified methods of nanoparticles synthesis in pH-sensitive nano-carriers production for doxorubicin delivery on MCF-7 breast cancer cell line. Int J Nanomedicine. 2019;14:3615-27.
 28. Mailafiya MM, Moklas MAM, Abubakar K, Danmaigoro A, Chiroma SM, Rahim EBA, et al. Cytotoxicity Studies of Curcumin Loaded-cockle Shell-derived Calcium Carbonate Nanoparticles. Nanoscience & Nanotechnology-Asia. 2021;11(1):35-41.
 29. Danmaigoro A, Selvarajah GT, Noor MHM, Mahmud R, Zakaria MZAB. Development of Cockleshell (*Anadara granosa*) Derived CaCO₃ Nanoparticle for Doxorubicin Delivery. Journal of Computational and Theoretical Nanoscience. 2017;14(10):5074-86.
 30. Hammadi NI, Abba Y, Hezmee MNM, Razak ISA, Jaji AZ, Isa T, et al. Formulation of a Sustained Release Docetaxel Loaded Cockle Shell-Derived Calcium Carbonate Nanoparticles against Breast Cancer. Pharmaceutical Research. 2017;34(6):1193-203.
 31. Jasim AJ, Sulaiman GM, Ay H, Mohammed SA, Mohammed HA, Jabir MS, et al. Preliminary trials of the gold nanoparticles conjugated chrysin: An assessment of anti-oxidant, anti-microbial, and in vitro cytotoxic activities of a nanoformulated flavonoid. 2022;11(1):2726-41.
 32. Khashan KS, Sulaiman GM, Hussain SA, Marzoog TR, Jabir MSJJoI, Polymers O, et al. Synthesis, characterization and evaluation of anti-bacterial, anti-parasitic and anti-cancer activities of aluminum-doped zinc oxide nanoparticles. 2020;30(9):3677-93.
 33. Hadi NA, Mahmood RI, Al-Saffar AZ. Evaluation of antioxidant enzyme activity in doxorubicin treated breast cancer patients in Iraq: A

molecular and cytotoxic study. *Gene Reports*. 2021;24.

34. Al-Ziaydi AG, Al-Shammari AM, Hamzah MI, Kadhim HS, Jabir MS. Newcastle disease virus suppress glycolysis pathway and induce breast cancer cells death. *Virusdisease*. 2020;31(3):341-8.

35. Al-Ziaydi AG, Al-Shammari AM, Hamzah MI, Jabir MSJCCI. Hexokinase inhibition using D-Mannoheptulose enhances oncolytic newcastle disease virus-mediated killing of breast cancer cells. 2020;20(1):1-10.

36. Ibrahim AA, Kareem MM, Al-Noor TH, Al-Muhimeed T, AIObaid AA, Albukhaty S, et al. Pt (II)-thiocarbohydrazone complex as cytotoxic agent and apoptosis inducer in Caov-3 and HT-29 Cells through the P53 and caspase-8 pathways. 2021;14(6):509.

37. Khashan KS, Jabir MS, Abdulameer FA. Carbon Nanoparticles Prepared by Laser Ablation in Liquid Environment. *Surface Review and Letters*. 2019;26(10).

38. Al-Shammari AM, Al-Saadi H, Al-Shammari SM, Jabir MS, editors. Galangin enhances gold nanoparticles as anti-tumor agents against ovarian cancer cells. *AIP Conference Proceedings*; 2020: AIP Publishing LLC.

39. Sameen AM, Jabir MS, Al-Ani MQ, editors. Therapeutic combination of gold nanoparticles and LPS as cytotoxic and apoptosis inducer in breast cancer cells. *AIP Conference Proceedings*; 2020: AIP Publishing LLC.

40. Al-Musawi S, Albukhaty S, Al-Karagoly H, Sulaiman GM, Jabir MS, Naderi-Manesh HJAINSN, et al. Dextran-coated superparamagnetic nanoparticles modified with folate for targeted drug delivery of camptothecin. 2020;11(4):045009.

41. Al-Ziaydi AG, Hamzah MI, Al-Shammari AM, Kadhim HS, Jabir MS, editors. The anti-proliferative activity of D-mannoheptulose against breast cancer cell line through glycolysis inhibition. *AIP Conference Proceedings*; 2020: AIP Publishing LLC.

42. Ramadin Y, Abdallah MA-H, Ahmad M, Zihlif A, Al-Ani SKJ, Al-Ani SGK. Optical properties of epoxy-glass microballoons composite. *Optical Materials*, . 1996;5(1-2):69-73.

43. Alves HWL, AFMCS, EAC, MJVB, Anjos aVCd. Structural, electronic and vibrational properties of the calcite phase of CaCO₃: An experimental and theoretical study 2011;5.

44. Wu J, Zhu YJ, Cao SW, Chen F. Hierarchically nanostructured mesoporous spheres of calcium silicate hydrate: surfactant-free sonochemical synthesis and drug-delivery system with ultrahigh drug-loading capacity. *Adv Mater*. 2010;22(6):749-53.

45. Zhang R, Xing R, Jiao T, Ma K, Chen C, Ma G, et al. Carrier-Free, Chemophotodynamic Dual Nanodrugs via Self-Assembly for Synergistic Antitumor Therapy. *ACS Appl Mater Interfaces*. 2016;8(21):13262-9.

46. Islam KN, Bakar MZBA, Noordin MM, Hussein MZB, Rahman NSBA, Ali ME. Characterisation of calcium carbonate and its polymorphs from cockle shells (*Anadara granosa*). *Powder Technology*. 2011;213(1-3):188-91.

47. Naka K, Huang SC, Chujo Y. Formation of stable vaterite with poly(acrylic acid) by the delayed addition method. *Langmuir*. 2006;22(18):7760-7.

48. Laifeng Wang, Ivan Sondi, Matijević aE. Preparation of Uniform Needle-Like Aragonite Particles by Homogeneous Precipitation *Journal of Colloid and Interface Science*. 1999;218:545-53.

49. McNeil SE. [Methods in Molecular Biology] Characterization of Nanoparticles Intended for Drug Delivery. 2011;697.

50. Islam KN, Zuki ABZ, Ali ME, Bin Hussein MZ, Noordin MM, Loqman MY, et al. Facile Synthesis of Calcium Carbonate Nanoparticles from Cockle Shells. *Journal of Nanomaterials*. 2012;2012:1-5.

51. Horie M, Nishio K, Kato H, Endoh S, Fujita K, Nakamura A, et al. Evaluation of cellular influences caused by calcium carbonate nanoparticles. *Chem Biol Interact*. 2014;210:64-76.

52. Kim MJ, Kim KM, Kim J, Kim KN. BMP-2 promotes oral squamous carcinoma cell invasion by inducing CCL5 release. *PLoS One*. 2014;9(10):e108170.